

## Alongwind Dispersion—A Simple Similarity Formula Compared with Observations at 11 Field Sites and in One Wind Tunnel

STEVEN R. HANNA AND PASQUALE FRANZESE

*School of Computational Sciences, George Mason University, Fairfax, Virginia*

(Manuscript received 23 August 1999, in final form 17 December 1999)

### ABSTRACT

Observations of alongwind dispersion of clouds were collected from 11 field sites and from one wind tunnel and were used to test simple similarity relations. Because most of the observations consist of concentration time series from fixed monitors, the basic observed variable is  $\sigma_t$ , the standard deviation of the concentration time series. The observed  $\sigma_t$ s range from 0.3 to 9000 s. The concentration time series observations also allow the travel time  $t$  from source to receptor to be estimated, from which the cloud advective speed  $u_e$  can be determined. Observed  $t$ s range from 2 to 40 000 s, and observed  $u_e$ s range from 0.5 to 16 m s<sup>-1</sup>. The alongwind dispersion coefficient  $\sigma_x$  is then calculated from  $u_e \sigma_t$ . The resulting  $\sigma_t$  and  $\sigma_x$  observations support the similarity relations  $\sigma_t = 0.1t$  and  $\sigma_x = 2u_* t$ , where  $u_*$  is friction velocity. About 50% of the observations are within a factor of 2 of these similarity relations.

### 1. Introduction

Models for the transport and dispersion of instantaneous or transient releases such as puffs or instantaneous line sources must be able to parameterize the alongwind dispersion coefficient  $\sigma_x$  and the effective speed  $u_e$  at which the cloud is moving. In the case of releases near the ground,  $u_e$  will increase as the cloud moves downwind, because the cloud's vertical size will continually increase. Although there are several similarity-based theoretical models of alongwind dispersion available (e.g., Chatwin 1968; Wilson 1981; van Ulden 1992), there are very few field datasets that can be used for model development and evaluation.

Several high-quality puff- or instantaneous line source–dispersion experiments have been carried out during the past few years, and the data are now becoming available. In each of these cases, the release was in the layer within 100 m of the ground. These new data have been combined with several sets of older data, including puff releases near the ground and instantaneous crosswind line releases at elevations of about 100–200 m, to determine whether the data follow some simple similarity relations. This paper describes the theoretical background for alongwind dispersion, reviews the experiments, presents some tables and figures of the

key observations, and suggests some simplified formulas for  $\sigma_x$ .

### 2. Theoretical considerations and methods of analysis

#### a. Definition of $\sigma_x$

Many current applied Gaussian models of puff dispersion (e.g., Sykes and Henn 1995; Sykes et al. 1996) make use of the alongwind dispersion coefficient. In the context of the Gaussian formula, it refers to a bulk standard deviation of the concentration distribution over the entire puff at any given time. However, in field or wind tunnel experiments, the  $\sigma_x$  observations nearly always represent observations at a given height above the surface made by a fixed monitor or by an aircraft. In some experiments, in which several monitors are located along a crosswind sampling line, it is possible to calculate the puff's  $\sigma_x$  for crosswind-averaged concentrations at a given height. Another kind of  $\sigma_x$  observation is a single monitor observing the cloud from an instantaneous line source release. In all these practical cases, representing several reasonable methods of interpreting and calculating the “observed”  $\sigma_x$ , it is obvious that the observed  $\sigma_x$  must be an underestimate of the bulk cloud  $\sigma_x$ , because observations at a single height cannot fully account for the effects of wind shear tilting. Nevertheless, these various kinds of  $\sigma_x$  observations are grouped together in this analysis, with the justification that the differences in the resulting observed  $\sigma_x$ s are minor.

For fixed monitors on crosswind sampling lines, there

---

*Corresponding author address:* Dr. Steven R. Hanna, CSI MS 5C3, 103 Science and Technology I, George Mason University, 4400 University Drive, Fairfax, VA 22030-4444.  
E-mail: shanna@gmu.edu

is insufficient coverage by monitors to calculate  $\sigma_x$  directly. Instead, the time series of concentration at single monitors is used to calculate  $\sigma_t$ , which is the standard deviation of concentration distribution over time. Then,  $\sigma_x$  is estimated from  $u_e \sigma_t$ .

### b. Basic similarity formulas and assumptions

As has been known for almost 50 years (Taylor 1953), dispersion is influenced by the mean wind shear as well as the turbulence. The early theoretical analyses were concerned with both the alongwind component of dispersion  $\sigma_x$  as well as the crosswind component of dispersion  $\sigma_y$ . The wind velocity in the boundary layer nearly always has a directional shear that averages about 30° over a depth of several hundred meters, because of the balance of pressure, Coriolis, and drag forces. The contribution of wind directional shear to  $\sigma_y$  becomes significant for puffs that have been transported for distances that are large enough that the puff's vertical size is a significant fraction of the boundary layer depth (Smith 1965).

In the surface boundary layer, within about 100 m of the ground, the alongwind speed shear is much larger than the directional shear, and therefore puffs are usually observed to be elongated in the  $x$  direction (more cigar shaped than spherical). Also, the alongwind speed shear may cause a tilt of the cloud centerline with respect to the vertical, which can also usually be observed visually. The total longitudinal variance of a puff can be obtained as the sum of the variance due to the tilt of the puff and the variance due to dispersion.

A thorough discussion of these effects is given by van Ulden (1992), who bases his derivation of  $\sigma_x$  on the continuity equation for the transport and dispersion of a passive cloud. He solves a differential equation containing eddy diffusivity coefficients. The eddy diffusivities and the wind speed profile are specified in terms of Monin–Obukhov similarity theory, and the local mass fluxes are written in terms of the gradient transfer assumption. The horizontal components of the turbulence are assumed to be homogeneous. The average horizontal relative alongwind eddy diffusivity is parameterized as  $K_x = \alpha \sigma_d \sigma_u$ , where  $\alpha$  is an empirical constant assumed to equal 0.3,  $\sigma_d$  is the component of  $\sigma_x$  due to dispersion, and  $\sigma_u$  is the standard deviation of the wind fluctuations in the alongwind direction. A similar parameterization is used for the relative crosswind eddy diffusivity  $K_y$ . Therefore,  $K_x$  and  $K_y$  grow as the cloud grows. The contribution to the total  $\sigma_x^2$  due to the tilt of the puff axis is expressed by the “centroid variance.”

Simple theoretical formulas for calculating the effects of alongwind or crosswind shears on  $\sigma_x$  or  $\sigma_y$ , respectively, are described by Saffman (1962), Smith (1965), Chatwin (1968), Pasquill (1969), Csanady (1969), and Wilson (1981). Wilson (1981) suggests the following formula:

$$\sigma_x^2 = \sigma_{xt}^2 + \sigma_{xs}^2, \quad (1)$$

where the first term represents the contribution due to alongwind velocity fluctuations and the second term represents the contribution due to the interaction of wind shear with vertical dispersion. The alongwind velocity fluctuation  $\sigma_u$  is known to equal about  $2u_*$ , where  $u_*$  is the friction velocity. It is convenient to express the two terms in Eq. (1) as follows:

$$\sigma_{xt} = Au_* t \quad \text{and} \quad (2)$$

$$\sigma_{xs} = B(1/\sqrt{12})\sigma_z(du/dz)t, \quad (3)$$

where  $u$  is the mean wind speed,  $z$  is the height, and  $A$  and  $B$  are constants that can be initially assumed to be of order unity and can be “calibrated” with data. The form of Eq. (3) is taken directly from Smith (1965). The factor of  $1/\sqrt{12}$  is a conversion factor that equals the standard deviation of a uniform distribution of width one.

The shear component in Eq. (3),  $\sigma_{xs}$ , is seen to be the product of the vertical dispersion  $\sigma_z$  and the wind shear  $du/dz$ . Wind shear alone can only increase the tilt of the puff and cannot contribute to puff dispersion in the absence of  $\sigma_z$ . The shear component does not vary as much with stability as expected, because  $\sigma_z$  and  $du/dz$  tend to be negatively correlated (i.e., in convective conditions,  $\sigma_z$  would be large and  $du/dz$  would be small, and in stable conditions, the reverse would be true).

The theoretical analyses by Chatwin (1968) and Wilson (1981) are based to some extent on similarity theory, and both lead to a general agreement that the total  $\sigma_x$  is approximately equal to a constant times  $u_* t$ :

$$\sigma_x = Du_* t, \quad (4)$$

where the constant  $D$  is estimated to be somewhere between 1 and 3. This same simple formula can be derived from van Ulden's (1992) model by assuming neutral conditions and other simplifications.

There are several ways to derive Eq. (4) from Eqs. (1)–(3), but the simplest is to assume a ground-based puff in Eq. (3), for which  $\sigma_z$  equals a constant times the mass-mean height  $z_m$  of the puff (for Gaussian distributions, this constant is about 1.7). Then further assume that the atmosphere is neutral, for which  $du/dz$ , at the height  $z_m$ , equals  $u_*/(0.4z_m)$ . Consequently,  $\sigma_z(du/dz)$  is proportional to  $u_*$ , and  $\sigma_{xs}$  is proportional to  $u_* t$ , which is the same functional form as the first (turbulent component) term in Eq. (2). Therefore the sum of the two terms equals a constant times  $u_* t$ .

Despite the apparent simple result given for  $\sigma_{xs}$  in the above derivations, it is important to note that the influence of the mean wind shear is difficult to parameterize in the boundary layer, because the wind shear is a strong (inverse) function of height. For example,  $du/dz$  is 10 times as large at a height of 2 m as it is at a height of 20 m. The “constant” in Eq. (4) should be calibrated with data.

c. Analysis of concentration time series to derive effective cloud speed and  $\sigma_t$

For the “historical” field experiments for which the data are presented in tables in reports and the detailed concentration time series are no longer available, we used the original authors’ estimates of the basic variables such as  $\sigma_x$ ,  $\sigma_t$ , and  $u_e$ . For field experiments for which key variables were not already calculated by the original authors and the detailed data were still available, we derived these basic variables.

In nearly all field experiments, the cloud observations are made by fixed concentration monitors, installed at elevations of a few meters and oriented in nearly equally spaced groups of monitors in the crosswind direction at a few downwind distances. Thus  $\sigma_x$  cannot be directly calculated because of an insufficient number of monitors in the alongwind direction. Instead, the observed time series of concentration (usually given as 1-s averages) are first used to estimate  $\sigma_t$ . For some experiments with limited numbers of crosswind samplers, this procedure is done with data from a single monitor. For other experiments with extensive arrays of crosswind samplers, the crosswind averaged concentration  $C_y$  is estimated before calculating  $\sigma_t$ .

The effective speed of the cloud was also calculated for many of the datasets. If high-resolution observations of horizontal and vertical profiles of concentration and wind speed were available at a field site,  $u_e$  could be calculated directly via a concentration-weighted integration of the puff [ $u_e = (\int uC dx dy dz)/(\int C dx dy dz)$ , where  $C$  is the three-dimensional concentration distribution]. However, these detailed three-dimensional data are not available in the analyzed datasets. The simple approximation could also be used that  $u_e$  equals the wind speed at the mass-mean height  $z_m$  of the cloud. This height can be considered to be equal to about  $0.6\sigma_z$  for ground-based clouds. However, the exact value of the constant, 0.6, is open to discussion (e.g., see Wilson 1981).

The effective speed of the cloud can also be directly estimated from the  $C(t)$  or  $C_y(t)$  observations based on knowledge of the time between the cloud release and the arrival of the center of the cloud at the monitor. It is important to note that, in this case,  $u_e$  is not a local value (as desired for use in the equation  $\sigma_x = u_e\sigma_t$ ) but represents an average  $\bar{u}_e$  over the total path of the cloud. For the purposes of this analysis, it is desired that the average  $\bar{u}_e$  not depart from the local  $u_e$  by more than about 10%. To determine whether this 10% criterion is satisfied for these datasets, we estimated the magnitude of the ratio  $\bar{u}_e/u_e$  for neutral conditions near the ground using a logarithmic wind profile,  $0.4u_e/u_* = \ln(z_m/z_0)$ , where  $z_0$  is the surface roughness length and  $z_m$  is the mass-weighted average height of the cloud. It is further assumed that the cloud has an initial average height  $z_{mi}$  and that the cloud’s subsequent growth in  $z_m$  follows similarity theory:

$$z_m = z_{mi} + 0.4u_*t. \quad (5)$$

Then the ratio  $\bar{u}_e/u_e$  can be calculated from the definition of  $\bar{u}_e = (1/t) \int_0^t u_e dt'$ , where  $t$  is the travel time to the monitoring line. The solution is given below:

$$\bar{u}_e/u_e = 1 + [a/(bt)] - \{1 + [a/(bt)] \ln a\} / \ln(a + bt), \quad (6)$$

where  $a = z_{mi}/z_0$  and  $b = 0.4u_*/z_0$ . The solution to this equation has been plotted for a range of values of  $a$  and  $b$  typical of those observed during the field experiments being analyzed, with the result that the ratio  $\bar{u}_e/u_e$  is usually predicted by Eq. (6) to be about 0.9. For a small number of the field trials, for which  $z_{mi}/z_0$  is close to unity,  $\bar{u}_e/u_e$  is predicted to be about 0.7–0.8 at the location of the monitors. Thus the difference can be neglected for these field datasets without much effect on the results.

Given the estimate of  $u_e$ ,  $\sigma_x$  is calculated from the expression  $u_e\sigma_t$ . The standard deviation  $\sigma_t$  has been calculated using several alternate methods, depending on the data that are available. For example, the standard second-moment method is used if high-resolution concentration time series  $C(t)$  are available and the data are smoothly varying. However, in the case of non-Gaussian distributions (e.g., with outliers, or two or more distinct peaks), the second-moment method is sometimes less appropriate. For these cases, the concentration time series is scanned to identify the time interval  $dt_{0.1}$  between the times when the concentration first rose above  $C_{\max}/10$  and last dropped below  $C_{\max}/10$ , and  $\sigma_t$  is calculated as  $dt_{0.1}/4.3$ , where the 4.3 is consistent with a Gaussian distribution. For a few of the field trials with missing or unreliable data at lower concentrations, the time interval  $dt_{0.5}$  between the two times corresponding to  $C_{\max}/2$  is identified, and  $\sigma_t$  is calculated as  $dt_{0.5}/2.4$ , where the 2.4 is consistent with a Gaussian distribution. For other experiments for which detailed  $C(t)$  data are not available but for which the time duration  $T_d$  that the cloud is over the monitor is reported in tables or plotted in figures,  $\sigma_t$  is calculated as  $T_d/4.3$ . Note that this latter method is similar to the  $dt_{0.1}/4.3$  method. For a few experiments for which no  $C(t)$  or  $T_d$  data are reported and for which the only  $\sigma_t$  data available are points in published plots, the  $\sigma_t$  values are scaled visually from the figures.

Note also, as discussed in section 2a, that the preferred basic dataset at a given downwind distance would consist of a  $y$ - $z$  cross section of averaged concentrations. However, such integrated data are not available in any of the experiments. In a few experiments, there are available crosswind-summed concentrations, which help to average out the effects of internal puff variability and horizontal wind shears. However, if the puff trajectory was not perpendicular to the monitoring line, the concentration time series recorded by each monitor on the line had to be corrected to account for the delay or offset between the arrival times at the various monitors. For

a few other experiments, the crosswind coverage of the monitors was limited, and concentration time series from single monitors had to be used to calculate  $\sigma_t$ . The net result of these limitations imposed by the experimental procedures is that the gross cloud  $\sigma_t$  and  $\sigma_x$  are probably underestimated; nevertheless we proceed with the analysis under the assumption that these differences are small.

*d. Cloud distortion at large distances and simple estimates of horizontal dispersion*

Many of the field datasets analyzed in this paper involve puff- or instantaneous line-source dispersion over timescales of several hours and over distances of 10 km or more, which can be thought of as mesoscale times and distances. As Gifford (1989) and Smith (1998) mention, contaminant clouds can become very convoluted at large times and distances because of the action of mesoscale wind fields, which tend to break up the cloud into streaks and patches with open spaces in between. This “breakup” of the cloud typically occurs at travel times of an hour or more. There is a continuous spectrum of horizontal turbulence that acts to maintain a near-linear increase of cloud width with time out to travel times of several days. It is remarkable that Heffter’s (1965) 35-year-old parameterization for puff lateral spread,

$$\sigma_y \text{ (in meters)} = (0.5 \text{ m s}^{-1})t \text{ (in seconds)}, \quad (7)$$

has proved to fit recent data very well. This simple relation fits Gifford’s (1995) compilation of  $\sigma_y$ -versus- $t$  data from nine field experiments almost as well as does the prediction of his random-force theory. The data from Gifford’s study cover  $\sigma_y$  from about 30 m to 200 km and travel times from about 30 s to 4 days.

After an hour or more of puff travel in a variable wind field, there is little to distinguish between the lateral dispersion parameter  $\sigma_y$  and the alongwind dispersion parameter  $\sigma_x$ . The cloud has been broken up by the wind field so that it is equally dispersed by turbulence and shears in all horizontal directions. There is no longer an obvious  $x$  and  $y$  direction; instead there is simply one radial  $\sigma_r$ , where  $r$  is the horizontal direction from the center of mass of the cloud or puff. Therefore Gifford’s (1995)  $\sigma_y$  data and Heffter’s (1965)  $\sigma_y$  formula can be considered to be equivalent to the alongwind dispersion component  $\sigma_x$  at mesoscale and larger scales. Furthermore, Gifford argues that the effects of wind shears are implicitly included in the observations, in his random force theory, and in Eq. (7) at mesoscale and larger scales.

Heffter’s (1965) linear  $\sigma_y$  formula, given as Eq. (7), can be written in the same form as Eq. (4) by assuming that the constant of  $0.5 \text{ m s}^{-1}$  is an average  $\sigma_v$  over the cloud trajectory, where  $\sigma_v$  is the standard deviation of lateral fluctuations in wind speed. Because  $\sigma_v$  is roughly equal to  $2u_*$  and because  $u_*/u$  is roughly equal to  $1/20$ ,

then Eq. (7) is consistent with an average friction velocity of approximately  $0.25 \text{ m s}^{-1}$  and an average wind speed of approximately  $5 \text{ m s}^{-1}$ , which are typical of the experimental conditions studied in the current paper. Furthermore, these assumptions, along with the assumptions that  $u_e = u$  and  $\sigma_t = \sigma_x/u_e$ , also lead to a simple linear proportionality between  $\sigma_t$  and  $t$ :

$$\sigma_t = 0.1t. \quad (8)$$

This simple formula will also be tested with the data from the field experiments.

### 3. Description of field experiments and wind-tunnel experiment

An attempt was made to acquire as many alongwind dispersion observations from as many sites as possible. The literature was surveyed, and several candidate datasets were identified in addition to the recent datasets that were available as part of ongoing research studies by the authors. Additional datasets were acquired for analysis based on information on the experiments available in reports and journal articles. A summary of the characteristics of the data from the 11 field sites and the wind-tunnel study is given in Table 1. Note that there are data available from over 120 puff- or instantaneous line-source field trials, from which over 650  $\sigma_t$  observations could be obtained using data from multiple monitoring arcs and from simultaneous measurements by ground-based samplers and airplanes. In most cases, the fundamental observations of concentrations were made by stationary monitors mounted on short towers near the ground and arrayed along cross wind lines.

The Dugway Proving Ground (DPG) (Biltoft 1997) Defense Threat Reduction Agency (DTRA) Phase-I puff trials were carried out to evaluate puff dispersion models such as Second-Order Closure Integrated Puff (SCIPUFF; Sykes et al. 1996), which typically predict the “ensemble” mean concentration. Each ensemble was generated in the experiment by releasing a number (2–35) of puffs during similar conditions. For each of the 23 ensemble trials, the mean concentration time series was calculated using the 2–35 individual time series. The puffs, with initial diameters less than about 1 m, were released near ground level, and the underlying surface was a flat desert with some vegetation. The single sampling line was located a few hundred meters downwind of the source (in practice, the sampling line was fixed and the downwind distance from source to sampling line was varied by moving the source). The  $\sigma_t$  calculations were based on the second-moment method applied to the time series of crosswind-summed concentrations. Extensive turbulence observations were made at the field site and used to calculate  $u_*$  and the Monin–Obukhov length  $L$  by Biltoft (1997). The Monin–Obukhov length is proportional to  $u_*^3$  divided by the turbulent heat flux. Here  $L$  is an indication of boundary layer stability and is reported for the various experi-

TABLE 1. Summary of alongwind dispersion experiments, including source release characteristics (all nearly instantaneous), number of trials, monitoring distances, surface roughness length ( $z_0$ ), concentration variable being analyzed, wind speed reference height, wind speed ranges, and stability ranges. The symbol n/a means that the data are not available.

Experiment	Release elevation and type of source	No. of trials	Monitoring distances (m)	$z_0$ (mm)	Concentration variable being analyzed	Wind speed reference height (m)	Wind speed range ( $m s^{-1}$ )	Stability range
DTRA phase 1	Ground-level point source	23 ensembles, each consisting of about 10–20 releases	200, 300, 400, 800, 1200. (Fixed sampling line, varying release point.)	0.3	Crosswind-summed C (near ground)	2	2–7	Mostly unstable; some stable
Dipole Pride 26 daytime tests	Ground-level point source	10	~11 000	32	Crosswind-summed C (near ground)	10	3–5	Unstable
Dipole Pride 26 nighttime tests	Ground-level point source	5	~11 000	32	Crosswind-summed C (near ground)	10	2–5	Stable
Kit Fox ERP	Ground-level point source	6	225	200	Crosswind-summed C (near ground)	2	2–3	Neutral to stable
Kit Fox URA	Ground-level point source	9	225	20	Crosswind-summed C (near ground)	2	3–4	Neutral to stable
Kit Fox SSR	Ground-level point source	6	225	0.2	Crosswind-summed C (near ground)	2	2–3	Neutral to stable
Hanford Kr-85	Ground-level point source	6	200, 800	30	Crosswind-summed C (near ground)	1.5	1–8	Stable to unstable
LROD	90-m line source	11	~2500 to ~100 000	0.02–0.86	C at single monitor (near ground and aircraft)	10	3–11	Near neutral
OLAD	100-m line source and ground-level line source	3 aircraft and 8 surface	~1000 to ~25 000	30	C at single monitor (near ground and aircraft)	2	0.5–7	Near neutral
Marchwood wind tunnel	Ground-level point source	4 ensembles, each consisting of about 150–300 releases	1, 3, 5, 7	0.3	C at single monitor (near ground)	Free stream	1–4	Neutral
Victoria	91-m line source	17	43 000–185 000	40	C at single monitor (near ground)	Average between 30 and 90 m	3–15	n/a
Oceanside	61–152-m line sources and ground-level point sources	15	23 000	n/a	C at single monitor (near ground)	Average between 8 and 120 m	1–5	n/a
Fort Wayne	91–244-m line sources	34	1600–12 000	n/a	C at single monitor (near ground)	Release height	5–16	n/a
EAPJ	Ground-level point sources	22	1500–7000	n/a	C at single monitor (near ground)	n/a	n/a	Unstable to stable
SRDES	Ground-level point sources	21	20–100	n/a	C at single monitor (near ground)	Average between 0 and 6 m	1–2	n/a

ments in Table 2. However, we point out that  $L$  is not used as part of our similarity expressions for  $\sigma_x$  or  $\sigma_z$ .

The Nevada Test Site—Yucca Flat puff trials are known by the name Dipole Pride 26 (Biltoft 1998; Watson et al. 1998) and are broken down into day and night conditions in the subsequent analysis (“d. tests” and “n. tests” in the tables and figures). Figure 1 presents the terrain elevations at the site and the locations of the source, the sampling lines, the meteorological stations, and other instrumentation. The sampling line (line 2 in Fig. 1) with six fast-response sensors was located about 11 000 m from the source, which is an order of magnitude farther downwind than the monitoring distances at the DPG DTRA Phase-I site. This study was intended to provide data for testing puff models such as SCIPUFF over mesoscale distances in complex terrain with time- and space-varying wind fields. The source was near ground level (the puff centroids were carried by the exiting gas to a height of about 6 m), and the underlying surface was a desert with some brush. The initial diameter of the puffs was about 7 or 8 m. The calculations of  $\sigma_i$  are made using the second-moment method applied to the time series of crosswind-summed concentrations. A correction has been made to account for different arrival times at the various monitors on the sampling line, because of the relatively large (11 km) distance to the sampling line and because of the relatively large separation distance (about 1.5 km) of the monitors along the sampling line. In addition to the detailed concentration observations at the site, extensive meteorological data were collected at several locations along the puff trajectory. The mean wind velocity was calculated from sonic anemometer measurements;  $u_*$  and  $L$  were obtained from the report by Biltoft (1998). The mean wind velocity,  $u_*$ , and  $L$  values are given in Table 2.

The Nevada Test Site—Frenchman Flat experiments had the code name Kit Fox. Although the site is a flat desert, for the Uniform Roughness Array (URA) and for the Equivalent Roughness Pattern (ERP) trials, the investigators placed many rectangular plywood obstacles over a broad area in order to “roughen” the surface (Hanna and Steinberg 1996; Hanna and Chang 1999; Western Research Institute 1998). In the URA trials, the roughness elements were 20-cm tall, giving a roughness length of about 1 or 2 cm. In the ERP trials, there were 2.4-m roughness elements placed in the area within 35 m of the source, giving a roughness length of about 10 or 20 cm. In a third set of trials (the Smooth Surface Roughness, or SSR) described by Coulombe et al. (1998), the roughness elements were removed, leaving the smooth desert surface with a roughness length of about 0.02 cm. All experiments took place near sunset, as the wind speed was decreasing from about 5 to 2 m s<sup>-1</sup> and as the stability was changing from neutral to stable. The data from the URA, ERP, and SSR experiments were analyzed separately and are plotted on the figures with different symbols. For all sets of Kit Fox experiments, the dense carbon dioxide gas was released

from a 2.25-m<sup>2</sup> area source at ground level, and the duration of release was about 20 s. To minimize the effects of density and finite-duration releases as much as possible, the current study is restricted to the group of trials with higher wind speed (i.e., close to neutral conditions) and to the most distant (225 m) sampling line. In all cases,  $\sigma_i$  is calculated from time series of crosswind-summed concentrations, using the  $C_{\max}/10$  method described in section 2c. Onsite observations of  $u$ ,  $u_*$ , and  $L$  were available from sonic anemometers.

The Hanford Kr-85 experiments involved near-ground releases of puffs of krypton-85 tracer gas in a desert scrub environment on the grounds of the Battelle Pacific Northwest Laboratory (Nickola et al. 1970a,b). Two monitoring arcs were located at 200 and 800 m downwind, respectively. The  $\sigma_i$  estimates are based on our analysis of crosswind sums of concentrations, using the time series of  $C(t)$  tabulated in the original report. We applied the  $C_{\max}/10$  or  $C_{\max}/2$  methods, as described in section 2c. Initial puff diameters were less than 1 m. Detailed meteorological observations were also made, although the available data tables are limited. In particular, we had to estimate  $u_*$  based on the  $u_e$  observations at the two monitoring lines. For the expected roughness length, and the observed advective speeds, it was assumed that  $u_*/u_e = 0.1$  on each sampling line and the final  $u_*$  estimate was assumed to be the average of the two  $u_*$  values. The original reports included estimates of Pasquill stability class, which are given in Table 2 for the Hanford Kr-85 experiments.

Draxler (1979) summarized three U.S. Army along-wind dispersion studies from the 1960s. The Fort Wayne (Hilst and Bowne 1966), the Victoria (Smith and Miller 1966), and the Oceanside (Smith and Niemann 1969) experiments all involved elevated instantaneous line source releases from jet airplanes. The source elevations ranged from about 50 to 200 m. Of course, the release could not be truly instantaneous, because it took several minutes for the plane to traverse the release line. However, this release time was small in comparison with the travel time to the sampling lines, which were located several kilometers downwind (about 2–12 km at Fort Wayne, 40–180 km at Victoria, and 23 km at Oceanside). The Fort Wayne releases were just upwind of a moderate-sized city, and the Victoria and Oceanside releases were just offshore during onshore flows. Two different tracers, “large” 20- $\mu$ m particles and yellow fluorescent pigment, were used at Victoria and are analyzed separately. The initial diameters of the clouds were not reported but were probably about 10 m, corresponding to the diameter of the airplane wake. The  $\sigma_i$  estimates are based on concentration observations at single monitors (i.e., not crosswind sums). For the Fort Wayne and Oceanside experiments,  $\sigma_i$  was estimated from  $T_d/4.3$ , where  $T_d$  is the time that the cloud was present over the monitor and is tabulated in the original reports. For the Victoria experiments,  $\sigma_i$  was obtained by visually scaling data points in  $\sigma_i$ -versus-distance

TABLE 2. Modelers' data archive for all experiments analyzed. The data listed should be sufficient for reproducing the current results and for developing and testing alternate formulas for alongwind dispersion.

Test	Distance (m)	Release (local time)	Travel time (s)	u (m s <sup>-1</sup> )	u <sub>e</sub> (m s <sup>-1</sup> )	u <sub>w</sub> (m s <sup>-1</sup> )	L (m)	σ <sub>t</sub> (s)	σ <sub>x</sub> (m)	σ <sub>t</sub> /u <sub>w</sub> (s)	
DTRA Phase 1	T02	1802	27	5.6	7.0	0.26	-36	2.9	20.6	79.2	
	T01	1715	28	5.9	6.9	0.26	-18	2.9	20.1	77.3	
	T03	1900	33	4.6	5.8	0.2	-79	3.4	19.5	97.7	
	T09	1934	82	4.6	4.3	0.19	-207	7.4	31.8	168	
	T04	1844	82	3.6	3.6	0.16	-20	6.2	22.6	141	
	T08	1810	86	4.4	4.2	0.19	-18	7.6	31.5	166	
	T05	1900	95	3.6	3.7	0.2	-4	6.3	23.7	119	
	T07	1648	110	3.2	3.2	0.15	-3	7.5	24.4	163	
	T10	2044	110	3.4	3.2	0.16	226	10.2	33.1	207	
	T11	1105	110	7.4	7.4	0.34	-72	8.4	62.4	184	
	T12	1401	120	6.9	6.8	0.3	-25	8.5	58.0	193	
	T13	1542	156	4.5	5.0	0.21	-11	11.3	56.4	269	
	T06	1420	157	2.0	2.3	0.08	-0.4	13.0	29.5	369	
	T16	1421	167	7.1	7.2	0.32	-21	10.9	79.0	247	
	T14	1759	198	3.7	3.9	0.18	-34	16.5	64.3	357	
	T17	1923	216	5.1	5.5	0.25	133	18.0	99.8	399	
	T15	1854	271	2.7	2.9	0.11	74	24.5	70.1	638	
Dipole Pride 26	T162	1330	1634	5.1	6.8	0.36	-67	194	1319	3664	
	T122	1030	1741	7.1	7.6	0.5	-71	152	1149	2299	
	T171	1200	2331	4.9	4.7	0.34	-22	149	692	2034	
	T141	1300	2232	4.6	5.2	0.34	-28	163	846	2487	
	T161	1200	2570	4.8	4.2	0.34	-25	684	2889	8496	
	T121	0900	2491	5.1	5.3	0.4	-72	181	956	2391	
	T071	1300	2737	4.1	4.0	0.29	-24	151	596	2056	
	T072	1445	2975	4.4	3.6	0.27	-41	95	345	1278	
	T095	1400	3254	3.0	3.6	0.2	-46	131	467	2336	
	T111	1430	4054	3.2	3.0	0.2	-30	300	911	4557	
	T042	0538	2160	5.0	5.2	0.25	634	147	769	3074	
	T041	0400	2483	4.9	4.8	0.23	26	173	822	3572	
	T031	0400	2522	3.8	4.3	0.17	19	692	2948	17 339	
	T061	0400	4260	2.5	2.9	0.06	32	868	2508	41 792	
	T051	0440	4664	2.4	2.5	0.05	12	752	1849	36 988	
	KIT Fox ERP	5-1	Sunset	72	3.0	4.5	0.42	167	11.6	52.2	124
		3-2	Sunset	73	2.2	6.2	0.42	93	13.8	85.6	204
3-3		Sunset	91	2.0	4.0	0.4	74	16.0	64.0	160	
Kit Fox URA	3-1	Sunset	86	2.1	2.7	0.4	80	11.6	31.3	78	
	5-2	Sunset	89	2.3	4.6	0.42	99	13.8	63.5	151	
	5-5	Sunset	91	2.1	4.5	0.37	80	17.0	76.5	207	
	8-2	Sunset	68	4.2	5.0	0.34	159	4.0	20.0	58.8	
	6-2	Sunset	77	3.7	4.2	0.34	150	8.2	34.4	101	
	8-3	Sunset	77	3.6	4.8	0.34	194	4.0	19.2	56.5	
	6-1	Sunset	74	4.2	6.2	0.32	194	8.2	50.8	159	
	8-1	Sunset	91	4.3	4.8	0.35	203	6.9	33.1	94.6	
8-7	8-7	Sunset	65	3.0	3.7	0.27	80	10.5	38.9	144	
	8-4	Sunset	95	3.1	3.7	0.32	135	5.5	20.4	63.8	
	8-6	Sunset	75	3.4	3.9	0.27	93	14.9	58.1	215	
	8-3	Sunset	85	3.4	3.9	0.29	127	6.9	26.9	92.8	

TABLE 2. (Continued)

	Test	Distance (m)	Release (local time)	Travel time (s)	$u$ ( $m\ s^{-1}$ )	$u_e$ ( $m\ s^{-1}$ )	$u_w$ ( $m\ s^{-1}$ )	$L$ (m)	$\sigma_t$ (s)	$\sigma_x$ (m)	$\sigma_x/\sigma_u$ (s)
Kit Fox SSR	T09R03A3	225	1809	90	4	2.5	0.17	23	5.1	12.8	77.2
	T09R05A3	225	1820	103	3.3	2.2	0.13	12	6.6	14.3	108
	T09R06A3	225	1823	118	3.2	1.9	0.12	10	9.1	17.4	140
	T13R02A3	225	1815	122	2.8	1.8	0.11	8	5.7	10.5	96.5
	T13R04A3	225	1829	114	3.4	2	0.13	9	6.1	12.1	92.3
	T13R05A3	225	1830	107	3.7	2.1	0.15	10	7.4	15.6	106
	T2 arc 1	200	2300	391	1.3	0.5	0.08	Stab. Class: F	96	48	961
	T2 arc 2	800	2300	779	1.3	1	0.08	Stab. Class: F	172	172	1724
	T3 arc 1	200	0738	78	4.2	2.6	0.32	Stab. Class: D	12.4	32.2	124
	T3 arc 2	800	0738	213	4.2	3.8	0.32	Stab. Class: D	30	114	300
Hanford Kr-85	T5 arc 1	200	1052	38	8	5.2	0.62	Stab. Class: C	7.5	39	74.9
	T5 arc 2	800	1052	111	8	7.2	0.62	Stab. Class: C	13.8	99.4	138
	T6 arc 1	200	1130	40	7.3	5	0.59	Stab. Class: C	7.8	39	78.3
	T6 arc 2	800	1130	119	7.3	6.7	0.59	Stab. Class: C	13	87.1	117
	T7 arc 1	200	1052	62	4.6	3.2	0.36	Stab. Class: C	20.8	66.6	208
	T7 arc 2	800	1052	200	4.6	4	0.36	Stab. Class: C	19.7	78.8	197
	T8 arc 1	200	0602	174	1.5	1.1	0.14	Stab. Class: E	37	40.7	370
	T8 arc 2	800	0602	493	1.5	1.6	0.14	Stab. Class: E	92.5	148	925
	Test 1	59 776	0905	7812	2.6	7.7	0.10	-76	169	1304	13 583
	Test 2	4190-104 116	0710	755-10 382	8.2	10.5	0.29	-1667	26-179	271-1877	948-6563
LROD	Test 3	2478-108 464	1225	390-10 859	9.8	10.1	0.34	-1250	16-256	164-2590	480-7573
	Test 6	9746-101 894	0602	813-8956	7.7	10.7	0.27	-400	25-148	267-1579	985-5827
	Test 7	6981-105 766	1048	460-8642	9.3	12	0.33	-909	24-165	286-1979	880-6089
	Test 8	9155-102 674	1526	802-8473	10.3	12.7	0.36	370	17-137	212-1734	597-4885
	Test 9	3485-123 232	0716	260-12 645	10.3	10.1	0.36	-5000	17-347	167-3500	465-9749
	Test 10	25 669-113 191	0806	2345-11 141	5.1	9.9	0.18	455	65-373	645-3690	3665-20 966
	Test 11	11 386-98 747	1431	1104-9813	10.3	10.3	0.36	10 000	25-246	259-2531	723-7070
	Test 12	15 205-47 240	0700	1182-3595	11.3	13.5	0.39	625	43-135	575-1816	1471-4645
	Test 13	8933-100 416	1115	618-6551	11.3	15.6	0.39	476	16-304	245-4739	628-12 151
	251-1	1864-5498	0706	2220-6420	0.03-0.07	0.4-0.9	0.03-0.07	-20-100	595-1113	370-1000	12 333-16 667
OLAD	252-2	1622-22 400	0645	360-5120	2.9-3.7	4.4-5.9	0.27-0.34	100-1000	71-1170	320-5120	970-18 963
	254-4	9414-22 300	0656	960-2440	1.8-5.2	6.7-11.5	0.17-0.49	-1000-1000	93-502	915-3350	1867-19 706
	255-5	1639-7400	0658	1620-7300	0.9	1-1.3	0.09	-200-1000	405-1440	410-1460	4556-16 222
	258-6a	1623-26 400	0645	240-2700	5.7-6.8	6.8-12	0.54-0.65	1000	31-316	213-3090	394-5066
	258-6b	1623-26 400	0746	180-1920	5.7-6.7	7.5-11.2	0.54-0.63	100	24-147	215-1520	398-2413
	258-6c	1623-26 400	0830	160-1030	6.3-6.7	6.3-11.2	0.62	-1000	18-142	165-1380	940-2226
	260-9	1800-21 036	0648	2250-11 820	1.7-2.5	0.8-2.1	0.05-0.24	-50-100	163-1159	130-2063	2600-20 200
	261-10	900-11 100	0755	200-2950	1.7-3	2.1-4.7	0.16-0.29	-1000-1000	88-540	184-2553	1150-8803
	267-11	7600-15 500	0709	3240-9730	0.5	1.6-2.3	n/a	n/a	196-854	460-1360	n/a
	268-12	1616-5263	0400	2160-9240	0.5-0.8	0.6-0.7	0.04-0.07	17-25	564-3129	422-1782	6029-44 550
Fort Wayne	34 trials	1600-12 000	n/a	720-10 200	5-16	n/a	n/a	n/a	66-3060	n/a	n/a
	Test 1	48 000-178 000	1930	7500-26 100	5.8	5.9-6.8	0.20	n/a	840-4200	5376-28 644	26 880-143 218
	Test 2	134 000	1931	24 540	4.2	5	0.20	n/a	2520	13 760	68 802
	Test 3	48 000-176 000	1930	7200-38 700	5.2	3.2-8.6	0.10	n/a	2040-6000	13 600-38 306	136 000-383 059
	Test 4	43 000-182 000	1930	4500-30 300	5.6	4.1-12	0.20	n/a	1680-7740	13 072-56 768	65 360-283 838
Test 5	43 000-178 000	1930	7200-27 000	4.2	3.9-8.4	0.20	n/a	420-4140	2100-34 906	10 500-174 529	

These data are not here for each trial because several pages would be required

TABLE 2. (Continued)

Test	Distance (m)	Release (local time)	Travel time (s)	$u$ (m s <sup>-1</sup> )	$u_e$ (m s <sup>-1</sup> )	$u_x$ (m s <sup>-1</sup> )	$L$ (m)	$\sigma_t$ (s)	$\sigma_x$ (m)	$\sigma_x/u_x$ (s)
Test 6	43 000-174 000	1930	78 000-32 700	6.5	4-7.8	0.20	n/a	480-6000	1911-29 762	9556-148 810
Test 7	48 000-138 000	1915	8100-38 700	4.2	2.9-5.9	0.30	n/a	420-7020	1223-23 581	4077-78 602
Test 8	48 000-138 000	1915	9000-35 100	4.6	3.5-5.3	0.20	n/a	720-7020	3840-29 092	19 200-145 459
Test 9	43 000-185 000	1915	4500-33 300	6.6	4.1-12	0.20	n/a	1320-7980	6103-52 589	30 516-262 943
Test 10	48 000-134 000	1700	6600-29 700	6.9	4.3-7.5	0.40	n/a	540-7200	3391-40 000	8478-100 000
Test 11	7600-94 000	1700	24 300-31 200	6	3-3.8	0.30	n/a	2820-5700	8496-19 289	28 321-64 296
Test 12	48 000-174 000	1700	11 700-33 300	5.8	2.9-5.2	0.60	n/a	900-7020	3692-20 091	6154-33 485
Test 13	43 000-182 000	1700	3600-32 100	6.3	4.3-15	0.50	n/a	480-6000	3235-36 211	6470-72 421
Test 14	48 000-182 000	1700	6300-33 300	7.6	5.1-8.6	0.50	n/a	720-4320	5486-29 193	10 971-58 386
Test 15	85 000-178 000	1700	16 200-41 400	4.8	4.3-6.3	0.40	n/a	1800-5760	9444-36 814	23 611-92 035
Test 16	48 000-128 000	1700	8000-29 700	5.4	3.7-6.7	0.30	n/a	600-6600	3200-29 110	10 667-97 032
27	23 000	1757	12 105	2.4	1.9	n/a	n/a	321	875	n/a
28	23 000	1904	17 692	2.2	1.3	n/a	n/a	614	798	n/a
29	23 000	1906	20 909	1.5	1.1	n/a	n/a	1451	1596	n/a
30	23 000	1704	7667	3.4	3	n/a	n/a	237	712	n/a
31	23 000	1505	6970	3.8	3.3	n/a	n/a	363	1197	n/a
32y	23 000	1803	10 952	2.5	2.1	n/a	n/a	753	1582	n/a
32g	23 000	1803	10 000	2.5	2.3	n/a	n/a	879	2022	n/a
35y	23 000	1904	16 429	2	1.4	n/a	n/a	544	762	n/a
35g	23 000	1904	19 167	2	1.2	n/a	n/a	558	670	n/a
36y	23 000	1705	6970	2.9	3.3	n/a	n/a	209	691	n/a
36g	23 000	1705	6970	2.9	3.3	n/a	n/a	195	645	n/a
37y	23 000	1505	5349	5.4	4.3	n/a	n/a	251	1080	n/a
37g	23 000	1505	4792	5.4	4.8	n/a	n/a	112	536	n/a
38y	23 000	1705	6389	4.1	3.6	n/a	n/a	167	603	n/a
38g	23 000	1705	6571	4.1	3.5	n/a	n/a	251	879	n/a
M2	3400	1230-1330	1740	n/a	2.0	n/a	n/a	307	600	n/a
T2	2500	1500-1528	2940	n/a	0.9	n/a	n/a	447	380	n/a
T4	2500	1100-1130	810	n/a	3.1	n/a	n/a	321	991	n/a
T5	2500	1300-1330	2550	n/a	1.0	n/a	n/a	209	205	n/a
T5	5100	1300-1330	4350	n/a	1.2	n/a	n/a	363	425	n/a
W1	1500	1201-1227	1440	n/a	1.0	n/a	n/a	307	320	n/a
W1	5000	1201-1227	3960	n/a	1.3	n/a	n/a	642	810	n/a
W2	1500	1230-1300	600	n/a	2.5	n/a	n/a	84	209	n/a
W3	5000	1230-1300	1800	n/a	2.8	n/a	n/a	181	504	n/a
W5	1500	1230-1300	960	n/a	1.6	n/a	n/a	265	414	n/a
W6	1500	1230-1300	900	n/a	1.7	n/a	n/a	279	465	n/a
S2	3000	1411-1430	840	n/a	3.6	n/a	n/a	265	947	n/a
S2	7300	1411-1430	5040	n/a	1.4	n/a	n/a	209	303	n/a
O1	2600	1400-1430	660	n/a	3.9	n/a	n/a	140	550	n/a
O1	4700	1400-1430	2490	n/a	1.9	n/a	n/a	293	553	n/a
O2	2600	1400-1430	660	n/a	3.9	n/a	n/a	140	550	n/a
O2	4700	1400-1430	2790	n/a	1.7	n/a	n/a	433	729	n/a
O3	4700	1030-1100	4230	n/a	1.1	n/a	n/a	181	202	n/a

Oceanside

EAPJ

TABLE 2. (Continued)

Test	Distance (m)	Release (local time)	Travel time (s)	$u$ (m s <sup>-1</sup> )	$u_e$ (m s <sup>-1</sup> )	$u_c$ (m s <sup>-1</sup> )	$L$ (m)	$\sigma_t$ (s)	$\sigma_x$ (m)	$\sigma_x/u_c$ (s)
O6	2600	1000-1030	570	n/a	4.6	n/a	n/a	126	573	n/a
N1	6950	1607-1630	3810	n/a	1.8	n/a	n/a	377	687	n/a
N2	3450	1000-1030	2460	n/a	1.4	n/a	n/a	377	528	n/a
N2	6950	1000-1030	3960	n/a	1.8	n/a	n/a	335	588	n/a
N3	3450	1040-1110	1380	n/a	2.5	n/a	n/a	140	349	n/a
N6	6950	1530-1600	4650	n/a	1.5	n/a	n/a	181	271	n/a
Marchwood										
Pos 1	0.83	Indoor expt	2.1	1	0.51	0.047	Stab. Class: D	0.41	0.21	4.47
Pos 2	2.5	Indoor expt	5.5	1	0.6	0.047	Stab. Class: D	0.86	0.52	11.06
Pos 3	4.17	Indoor expt	8.4	1	0.64	0.047	Stab. Class: D	1.12	0.72	15.32
Pos 4	5.93	Indoor expt	11	1	0.69	0.047	Stab. Class: D	1.42	0.98	20.85
SRDES										
R-1	n/a	n/a	6	n/a	n/a	n/a	n/a	1.0	n/a	n/a
R-2	n/a	n/a	11	n/a	n/a	n/a	n/a	1.1	n/a	n/a
R-3	n/a	n/a	12	n/a	n/a	n/a	n/a	1.1	n/a	n/a
R-4	n/a	n/a	13	n/a	n/a	n/a	n/a	2.2	n/a	n/a
R-5	n/a	n/a	14	n/a	n/a	n/a	n/a	3.5	n/a	n/a
R-6	n/a	n/a	16	n/a	n/a	n/a	n/a	1.7	n/a	n/a
R-7	n/a	n/a	19	n/a	n/a	n/a	n/a	3.4	n/a	n/a
R-8	n/a	n/a	21	n/a	n/a	n/a	n/a	1.7	n/a	n/a
R-9	n/a	n/a	21	n/a	n/a	n/a	n/a	3.5	n/a	n/a
R-10	n/a	n/a	22	n/a	n/a	n/a	n/a	2.0	n/a	n/a
R-11	n/a	n/a	22	n/a	n/a	n/a	n/a	5.6	n/a	n/a
R-12	n/a	n/a	30	n/a	n/a	n/a	n/a	3.7	n/a	n/a
R-13	n/a	n/a	31	n/a	n/a	n/a	n/a	1.6	n/a	n/a
R-14	n/a	n/a	31	n/a	n/a	n/a	n/a	3.1	n/a	n/a
R-15	n/a	n/a	38	n/a	n/a	n/a	n/a	2.1	n/a	n/a
R-16	n/a	n/a	40	n/a	n/a	n/a	n/a	7.1	n/a	n/a
R-17	n/a	n/a	71	n/a	n/a	n/a	n/a	15	n/a	n/a
R-18	n/a	n/a	120	n/a	n/a	n/a	n/a	5.1	n/a	n/a

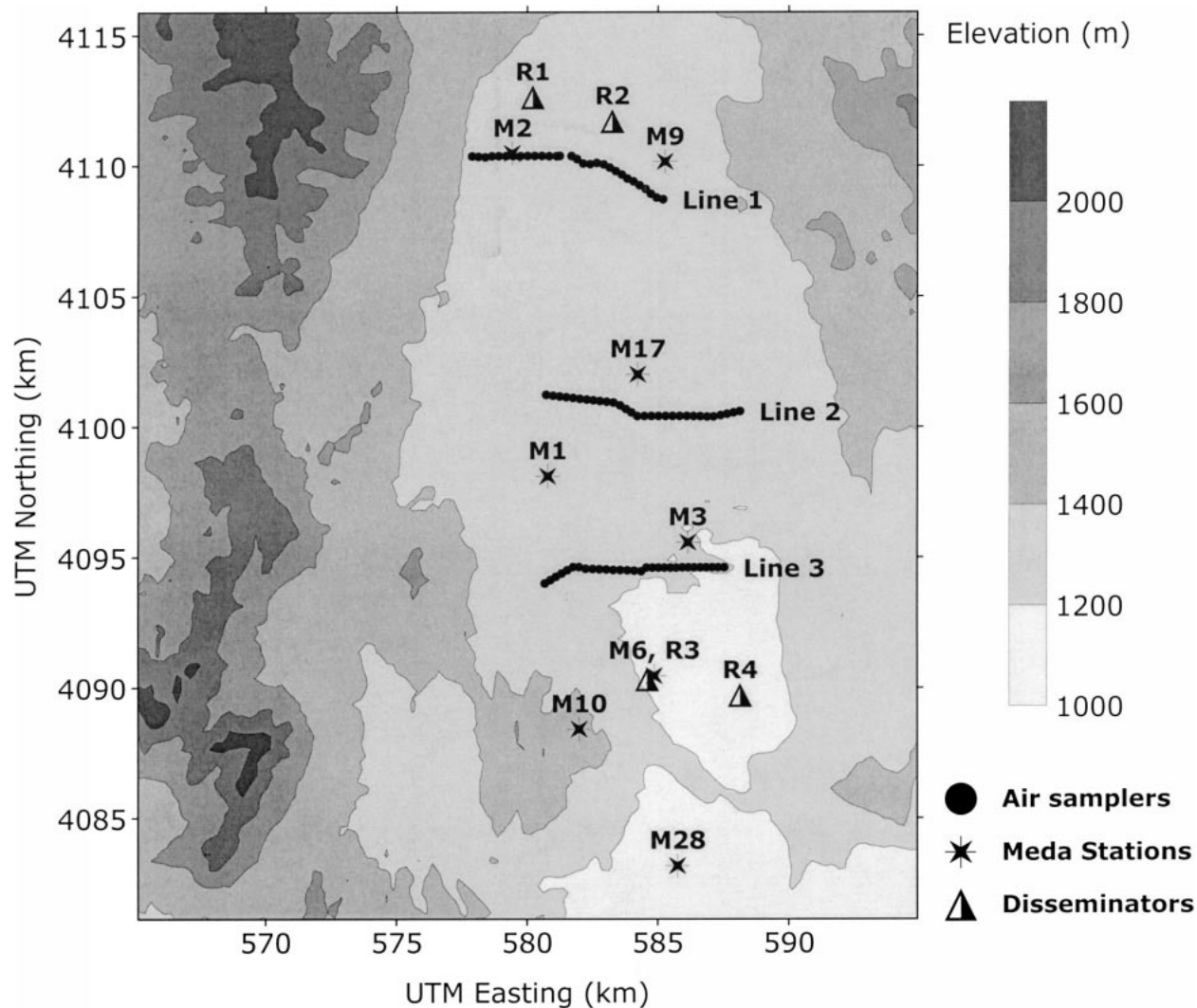


FIG. 1. Map of Dipole Pride 26 field site at Yucca Flat, Nevada Test Site (Biltoft 1998; Watson et al. 1998). Terrain contours are at 200-m separation, with dark shadings representing higher elevations. The releases took place at the “disseminator” locations marked as triangles. Meteorological observations were taken at “Meda” (meteorological data) stations marked as stars. Fifteen-minute average concentration observations were taken by air samplers, marked as circles, along three lines. The fast-response concentration observations analyzed in this paper were taken by six samplers along line 2.

plots in the original report. Meteorological observations such as mean wind speed are available in the data reports.

The Long-Range Overwater Dispersion (LROD) experiment (Bowers et al. 1994) was conducted within the overwater airspace of the Pacific Missile Range Facility, Kauai, Hawaii. It took place 30 years later than the three U.S. Army experiments described in the paragraph above but was similar in release type. The source was an instantaneous elevated (about 90 m) line source, with initial diameter of about 10 m, released from an airplane. Although concentration data were observed by both surface monitors (boats) and airplane monitors, few of the boat data were useful because of high seas. The airplane flew racetrack patterns across the cloud, centered on the

fixed longitudinal sampling line along which the boats were placed. The analysis treats the airplane and boat data separately. The original report included  $\sigma_x$  observations for single passes through the cloud by the airplane and  $\sigma_x$  estimates for single near-ground monitors. We calculate  $u_e$  based on the distance of the airplane or the monitor from the source and the arrival time of the cloud center-of-mass and used this  $u_e$  in the formula  $\sigma_t = \sigma_x/u_e$ . Extensive meteorological data are available in the report and in the project data archive (on CD-ROM).

The Over-Land Atmospheric Dispersion (OLAD) experiment (Biltoft et al. 1999) was very similar to the LROD experiment discussed in the paragraph above, except that the OLAD experiment took place “over land” at DPG, and that for some trials the instantaneous

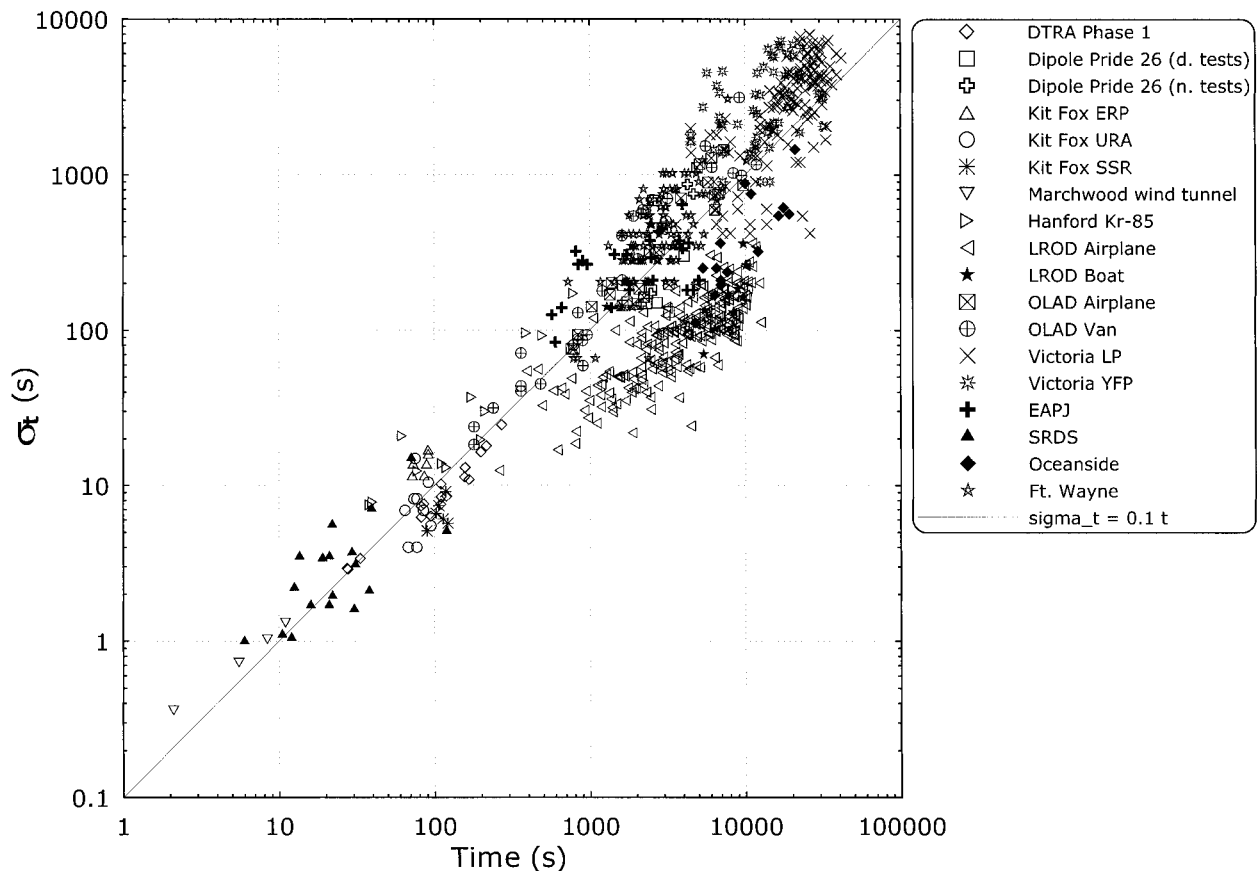


FIG. 2. Standard deviation of the observed concentration time series  $\sigma_t$ , plotted vs observed travel time  $t$  for all experiments. The different symbols are explained in the legend. The line represents the formula  $\sigma_t = 0.1t$ .

line source was released by an aircraft while for other trials it was released by a truck. Otherwise the experimental methods and the available data types were identical.

Sato et al. (1981) and Sato (1995) discuss their Short-Range Diffusion Experiment Series (SRDES), which involved near-ground releases of small puffs in a field, with monitoring mostly at a downwind distance of about 20 m. Monitors were also placed on a tower, so that vertical profiles of concentration could be obtained. For the SRDES experiments,  $\sigma_t$  was obtained by visually scaling data points from a plot of  $\sigma_t$  versus  $t$  in Sato et al. (1981). Extensive turbulence data were observed by sonic anemometers, although only limited data are presented in the references. Sato (1995) also presents data from the Environmental Assessment Program Japan (EAPJ) experiments, which involved the analysis of the leading and trailing edges of “detached plumes,” namely, plumes generated by finite duration (30 min–1 h) releases and observed at downwind distances of a few kilometers. For the EAPJ experiments, we calculated  $\sigma_t$  from the formula  $\sigma_t = T_d/4.3$ , where  $T_d$  is the reported time between the arrival of the leading edge of the cloud and the departure of the trailing edge, minus the duration of the initial release. Again, limited data are reported

in the journal articles and the full database is inaccessible.

The Marchwood wind-tunnel data (Robins and Fackrell 1998) focused on ensembles of short-duration releases of neutrally buoyant gas released at ground level in a neutral boundary layer (i.e., Pasquill stability class D). Conditions could be exactly replicated in the wind tunnel for each individual experiment of the ensemble. Very detailed time series of concentration measured at four distances downstream were obtained and analyzed by Robins and Fackrell (1998). We analyzed their reported values of  $\sigma_t$ ,  $\sigma_x$ , and  $u_*$  using the similarity theory discussed in section 2.

#### 4. Data summary and results

The data from the puff- and instantaneous line source trials at the 11 field sites and the Marchwood wind-tunnel experiment are summarized in the modelers’ data archive in Table 2, which contains the basic observations sufficient for similarity analysis of alongwind dispersion. The modelers’ data archive should be useful to other researchers in developing and testing their own theories. For some field sites, such as the LROD, OLAD, Fort Wayne, and Victoria sites, for which the datasets

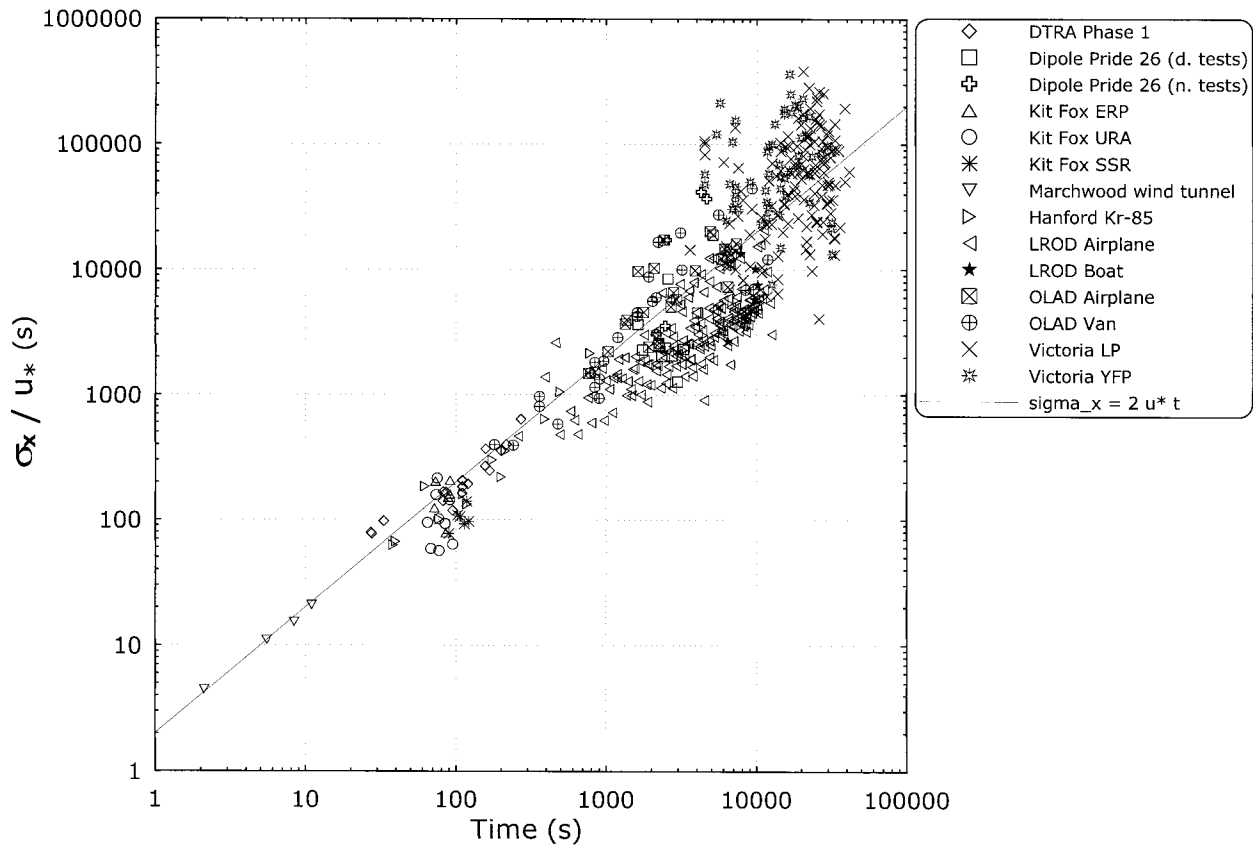


FIG. 3. Alongwind dispersion coefficient  $\sigma_x = u_e \sigma_t$ , divided by  $u_*$  and plotted vs  $t$  for the experiments listed in the legend. The different symbols are explained in the legend. The line represents the formula  $\sigma_x = 2u_* t$ .

are too large to include in Table 2, it will be necessary to refer to the data reports for additional data. For these sites, only the range of each variable is reported in Table 2. It should be mentioned again that, with the exception of the airplane data from the LROD and OLAD experiments for which  $\sigma_x$  was directly observed, the basic observations consist of puff  $\sigma_t$  and of travel time based on the observed time series of concentrations at each sampling line.

To test the similarity relations in Eqs. (4) and (8), it is interesting to present the combined data as plots of  $\sigma_t$  versus  $t$  and  $\sigma_x/u_*$  versus  $t$  in log–log format as in Figs. 2 and 3, respectively. The friction velocity was either observed directly by sonic anemometers or was derived from the cloud speed as described in section 3. Fortunately,  $u_*$  had been already included in the meteorological datasets of most of the experiments. About half of the points on the figures are within a factor of two of the simple linear relations given in Eq. (4), with the constant  $D$  equal to 2, and given in Eq. (8), with the same constant as derived in the paragraph above that equation. These equations are repeated below:

$$\sigma_t = 0.1t \quad \text{and} \quad (9a)$$

$$\sigma_x/u_* = 2t. \quad (9b)$$

The solutions to these equations are drawn as straight lines on the figures and are seen to provide good fits to the field and wind-tunnel data, which are from many different sites and which cover  $\sigma_t$  over four orders of magnitude (from about 0.3 to about 10 000 s) and travel times over four orders of magnitude (from about 2 to about 30 000 s or 8 h). The  $2u_*t$  relation is in good agreement with the theoretical prediction of Eq. (4) and prior analyses discussed in section 2.

The accuracy of the  $\sigma_x$  data in Fig. 3 depends on many parameters, such as the accuracy of the assumed puff advective speed, which is used to calculate  $\sigma_x = u_e \sigma_t$ , as discussed in section 2. The derivations in that section show that local  $u_e$  is likely to be within 10% of average  $\bar{u}_e$ . Uncertainties or biases in  $u_*$  can also contribute to displacement of points from the straight line in Fig. 3. For example, in the case of the mesoscale experiments, the locally observed  $u_*$  may not be representative of the average  $u_*$  over the entire cloud trajectory.

It is seen in Figs. 2 and 3 that certain groups of points, representing specific field trials, are displaced from the line of best agreement. In some cases, this displacement can be explained by the sampling methodology. For example, some  $\sigma_t$  observations are based on time series

of crosswind-summed concentrations, and some are based on time series of concentrations at a single point (intuition would suggest that the  $\sigma_t$  from the crosswind-summed data would be larger than the  $\sigma_t$  from the point data). The LROD and OLAD airplane  $\sigma_{x,s}$  are unique in that they are observed directly and not implicitly through  $\sigma_t$ . In other cases, the displacement of points on the figure may be due to fundamental physical causes such as biases in the  $u_*$  estimates. However, this same kind of scatter from one field experiment to another is always seen in field data, as shown by the plot of  $\sigma_y$  versus  $t$  for many independent field sites reported in Gifford's (1995) paper.

The disparity in numbers of points from one field experiment to the next hampers the visual inspection of Figs. 2 and 3. For example, there are dozens of points for the Victoria and LROD data but only a few points for Dipole Pride 26. It may be more meaningful to weight equally the data clusters from individual experiments rather than be influenced by the total number of points.

*Acknowledgments.* This research was sponsored by the Defense Threat Reduction Agency, with Major Thomas H. Smith as technical project monitor. Special assistance was received from Christopher Biltoft of the U.S. Army Dugway Proving Ground; Roland Draxler and Thomas Watson of the National Oceanic and Atmospheric Administration, Air Resources Laboratories; Junji Sato of the Meteorological Research Institute, Japan; Ian Sykes of Titan Corporation, ARAP Group; and Aad van Ulden of the Royal Netherlands Meteorological Institute. We also appreciate the assistance provided by Joseph Chang of George Mason University.

#### REFERENCES

- Biltoft, C., 1997: Phase I of DSWA transport and dispersion model validation study. DPG-FR-97-058, 156 pp. [Available from Meteorology and Obscurant Division, West Desert Test Center, U.S. Army Dugway Proving Ground, Dugway, UT 84022-5000.]
- , 1998: Dipole Pride 26: Phase II of DSWA transport and dispersion model validation study. DPG-FR-98-001, 130 pp. [Available from Meteorology and Obscurant Division, West Desert Test Center, U.S. Army Dugway Proving Ground, Dugway, UT 84022-5000.]
- , S. D. Turley, T. B. Watson, G. H. Crescenti, and R. G. Carter, 1999: Over-Land Atmospheric Dispersion (OLAD) test summary and analysis. WDTC Doc. WDTC/JCP-99/048, 38 pp. [Available from Meteorology and Obscurant Division, West Desert Test Center, U.S. Army Dugway Proving Ground, Dugway, UT 84022-5000.]
- Bowers, J. F., G. E. Start, R. G. Carter, T. B. Watson, K. L. Clawson, and T. L. Crawford, 1994: Experimental design and results for the Long-Range Overwater Diffusion (LROD) Experiment. DPG/JCP-94/012, 531 pp. [Available from Meteorology and Obscurant Division, West Desert Test Center, U.S. Army Dugway Proving Ground, Dugway, UT 84022-5000.]
- Chatwin, P. C., 1968: The dispersion of a puff of passive contaminant in the constant stress region. *Quart. J. Roy. Meteor. Soc.*, **94**, 350–360.
- Coulombe, W., J. Bowen, R. Egami, D. Freeman, D. Sheesley, J. Nordin, T. Routh, and B. King, 1998: Characterization of carbon dioxide releases—Experiment 2. Rep. 97-7240.1D, 173 pp. [Available from Desert Research Institute, University and Community College System of Nevada, P.O. Box 60220, Reno, NV 89506.]
- Csanady, G. T., 1969: Diffusion in an Ekman layer. *J. Atmos. Sci.*, **26**, 414–426.
- Draxler, R. R., 1979: Some observations of the along-wind dispersion parameter. *Proc. Fourth Symp. on Turbulence, Diffusion, and Air Pollution*, Reno, NV, Amer. Meteor. Soc., 5–8.
- Gifford, F. A., 1989: The shape of large tropospheric clouds, or “very like a whale.” *Bull. Amer. Meteor. Soc.*, **70**, 468–475.
- , 1995: Some recent long-range diffusion observations. *J. Appl. Meteor.*, **34**, 1727–1730.
- Hanna, S. R., and K. W. Steinberg, 1996: Studies of dense gas dispersion from short-duration transient releases over rough surfaces during stable conditions. *Air Pollution Modeling and Its Applications XI*, Plenum Press, 481–490.
- , and J. C. Chang, 1999: Testing of the HEGADAS model using the Kit Fox field data. *Proc. Int. Conf. and Workshop on Modeling the Consequences of Accidental Releases of Hazardous Materials*. San Francisco, CA, American Institute of Chemical Engineers, 229–246.
- Heffter, J. J., 1965: The variation of horizontal diffusion patterns with time for travel periods of one hour or longer. *J. Appl. Meteor.*, **4**, 153–160.
- Hilst, G. R., and N. E. Bowne, 1966: A study of the diffusion of aerosols released from aerial line sources upwind of an urban complex. Vols. I and II. Rep. DA-42-007-AMC-38(R), 231 and 583 pp. [Available from The Traveler's Research Center Inc., 250 Constitution Plaza, Hartford, CT 06103.]
- Nickola, P. W., J. D. Ludwick, and J. V. Ramsdell Jr., 1970a: An inert gas tracer system for monitoring the real-time history of a diffusing plume or puff. *J. Appl. Meteor.*, **9**, 621–626.
- , J. V. Ramsdell Jr., and J. D. Ludwick, 1970b: Detailed time-histories of concentrations resulting from puff and short-period releases of an inert radioactive gas: A volume of atmospheric diffusion data. BNWL-1272, UC-53, 193 pp. [Available from Battelle Memorial Institute, Pacific Northwest Laboratories, Battelle Boulevard, P.O. Box 999, Richland, WA 99352.]
- Pasquill, F., 1969: The influence of the turning of wind with height on crosswind diffusion. II. Meteorological aspects of air pollution. *Philos. Trans. Roy. Soc. London A*, **265**, 173–181.
- Robins, A. G., and J. E. Fackrell, 1998: An experimental study of the dispersion of short-duration emissions in a turbulent boundary layer. *Air Pollution VI*, C. A. Brebbia, C. F. Ratto, and H. Powers, Eds., WIT Press, 697–707.
- Saffman, P. G., 1962: The effect of wind-shear on horizontal spread from an instantaneous ground source. *Quart. J. Roy. Meteor. Soc.*, **88**, 382–393.
- Sato, J., 1995: An analytical study on longitudinal diffusion in the atmospheric boundary layer. *Geophys. Mag. Ser. 2*, **1**, 105–151.
- , F. Kimura, and T. Yoshikawa, 1981: The longitudinal spread of puff in the short range diffusion experiment. *Pap. Meteor. Geophys.*, **32**, 155–162.
- Smith, F. B., 1965: The role of wind shear in horizontal diffusion of ambient particles. *Quart. J. Roy. Meteor. Soc.*, **91**, 318–329.
- , 1998: Estimating the statistics of risk from a hazardous source at long range. *Atmos. Environ.*, **32**, 2775–2791.
- Smith, T. B., and R. L. Miller, 1966: Victoria diffusion trials. Vol. I. MRI-66-FR-374, 181 pp. [Available from Meteorological Research Inc., 464 West Woodbury Rd., Altadena, CA 91001.]
- , and B. L. Niemann, 1969: Shoreline diffusion program, Ocean-side, CA. Vols. I and II. MRI-64-FR-860, 230 and 456 pp. [Available from Meteorological Research Inc., 464 West Woodbury Rd., Altadena, CA 91001.]
- Sykes, R. I., and D. S. Henn, 1995: Representation of velocity gradient effects in a Gaussian puff model. *J. Appl. Meteor.*, **34**, 2715–2723.
- , S. F. Parker, and R. S. Gabruk, 1996: SCIPUFF—a gen-

- eralized hazard dispersion model. *Ninth Joint Conf. on the Applications of Air Pollution Meteorology*, Atlanta, GA, Amer. Meteor. Soc., 184–188.
- Taylor, G. I., 1953: Dispersion of soluble matter in solvent flowing slowly through a tube. *Proc. Roy. Soc. A*, **219**, 186–203.
- van Ulden, A. P., 1992: A surface-layer similarity model for the dispersion of a skewed passive puff near the ground. *Atmos. Environ.*, **26A**, 681–692.
- Watson, T. B., R. E. Keislar, B. Reese, D. H. George, and C. A. Biltoft, 1998: The DSWA Dipole Pride 26 field experiment. NOAA Tech. Memo. ERL ARL-225, 90 pp. [Available from NOAA Air Resources Laboratory ARL, R/E/AR, SSMC 3, Room 3151, 1315 East–West Highway, Silver Spring, MD 20910.]
- Western Research Institute, 1998: Final report on the 1995 Kit Fox Project. Vol. 1, Experimental description and data Processing, and Vol. 2, Data analysis for enhanced roughness test, Rep. WRI 98-7, 109 and 67 pp. [Available from WRI, 365 North Ninth St., Laramie, WY 82072-3380.]
- Wilson, D. J., 1981: Along-wind diffusion of source transients. *Atmos. Environ.*, **15**, 489–495.